Reaction Chemistry & Engineering

Kinetically Controlled Synthesis of Bimetallic Nanostructures by Flowrate Manipulation in a Continuous Flow Droplet Reactor

Journal:	*Reaction Chemistry & Engineering*
Manuscript ID	RE-COM-05-2018-000077.R1
Article Type:	Communication
Date Submitted by the Author:	23-Jun-2018
Complete List of Authors:	Santana, Joshua; Indiana University - Bloomington, Chemistry Koczkur, Kallum; Indiana University, Chemistry Skrabalak, Sara; Indiana University - Bloomington, Chemistry

Journal Name

COMMUNICATION

Kinetically Controlled Synthesis of Bimetallic Nanostructures by Flowrate Manipulation in a Continuous Flow Droplet Reactor

Received 00th January 20xx,
Accepted 00th January 20xx

DOI: 10.1039/x0xx00000x

www.rsc.org/

Joshua S. Santana, Kallum M. Koczkur, and Sara E. Skrabalak *

We show that different Au-Pd nanoparticles, ranging from sharp-branched octopods to core@shell octahedra, can be achieved by inline manipulation of reagent flowrates in a microreactor for seeded growth. Significantly, these structures represent different kinetic products, demonstrating an inline control strategy toward kinetic nanoparticle products that should be generally applicable.

Metal nanoparticles (NPs) have unique optical and chemical properties that arise from their composition, crystallite size, and shape,[1-3] allowing for diverse applications.[4-6] Bimetallic NPs similarly display size- and shape-dependent properties, where the specific bimetallic distribution contributes to their properties.[7] Nanostructures with different compositional (e.g., monometallic versus multimetallic) and structural features represent different kinetic and thermodynamic products and can be accessed through different synthetic conditions.[8-14] Thermodynamic products are the most stable, but kinetic products can be readily accessed through pathways with lower activation energies, with Wulff polyhedra representing the thermodynamic NP shape for face-centered cubic metals under idealized conditions.[15] Kinetic products deviate from this global minimum structure and typically arise in nanosyntheses when the deposition rate of adatoms is much faster the rate of adatom diffusion.[15] This condition kinetically traps atoms in high energy postions.[15] Seed-mediated co-reduction (SMCR) is a versatile method to synthesize multimetallic kinetic products.[16-19]

In SMCR, multiple metal precursors are co-reduced simultaneously in solution to deposit the metals on shape-controlled seeds.[18] For example, in a model Au-Pd system, a range of products were accessed by varying the pH of the reaction and metal precursors concentrations, including branched nanocrystals and more thermodynamically favorable core@shell nanocrystals.[20] This manuscript reports the synthesis of Au-Pd nanocrystals by SMCR but with a continuous flow microdroplet reactor, where kinetic control is achieved by inline manipulation of droplet pH and precursor concentrations through controlling relative flowrates. Significantly, this inline control strategy toward kinetic nanocrystal products should be generally applicable to other nanosyntheses, where the relative concentrations of precursors and reducing agent can be manipulated to tune the adatom addition rate relative to their surface diffusion rate.[15,23]

Microdroplet reactors are a way to synthesize large product volumes of nanomaterials through continuous production of uniform reaction droplets in a two-phase flow.[21] Microreactors offer advantages to batch reactions that include maintenance of thermal equilibrium within droplets, scale-up abilities for product volume, control of mass transport, and even *in situ* spectroscopic analysis through absorbance, fluorescence, and X-ray monitoring.[21-25] These conditions favor formation of highly uniform products and can give important mechanistic insight into nanomaterial formation. Even with the promise of microreactors, few nanosyntheses have been demonstrated with them and the utility of inline manipulation to access a variety of structures is largely unexplored.[26,27]

*Indiana University - Bloomington, Department of Chemistry, 800 E. Kirkwood Ave., Bloomington, IN 47405-7102 *E-Mail: sskrabal@indiana.edu*

Electronic Supplementary Information (ESI) available: experimental methods, results from control experiments. See DOI: 10.1039/x0xx00000x

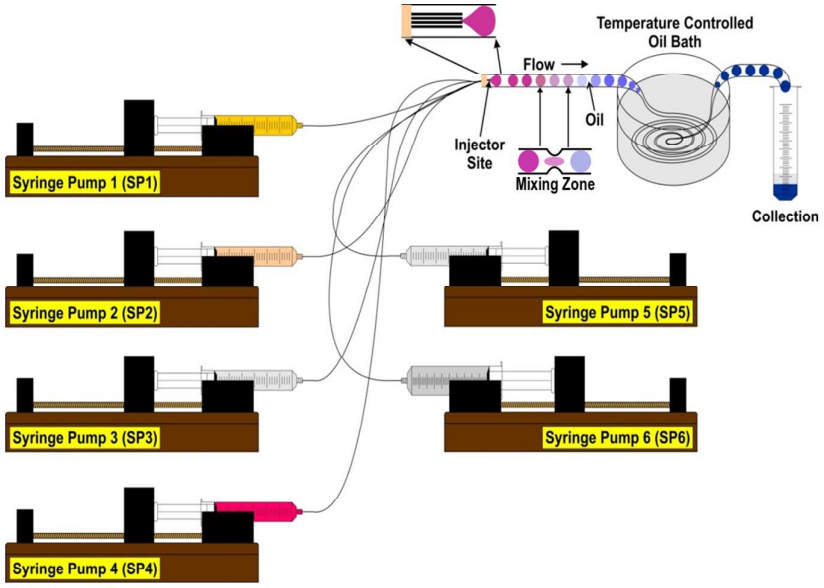

Figure 1. Schematic illustration of the microreactor used for continuous production of kinetically controlled NPs.

Recent studies showed that the relative flowrates of reagents in microdroplet reactors could be manipulated to achieve core@shell nanostructures with different shell thicknesses.[28] Also, different nanostructures have been synthesized inline by varying stock solutions as well as reaction temperature and/or residence time in flow reactors.[29-31] Now, we demonstrate that different bimetallic kinetic products can be readily accessed by SMCR through inline manipulation of relative flowrates of reagent solutions. This ability is demonstrated with the SMCR synthesis of shape-controlled Au-Pd NPs, with the flow approach being adapted from batch reactions where shapes were manipulated by varying the pH within the reaction droplets through the delivery of different amounts of hydrochloric acid (HCl).[20] Specifically, by adjusting the flow-rate of HCl relative to the flow-rate of the Au and Pd metal precursors, products that vary from sharply branched octopods to core@shell structures were possible. The microreactor confines the reactions into 10 µL droplets, with the carrier medium being injected at a rate of 1-2 times faster than the additive flowrate of the reagent materials to ensure uniform droplets.[32] These results demonstrate that nanomaterial shape can be manipulated inline by changing the relative flow-rates of reagent materials using a microreactor, without using the typical kinetic manipulation of changing temperature or residence time.

An illustration of the microreactor is in Figure 1 and was designed to reduce Au and Pd precursors simultaneously with L-ascorbic acid (L-aa) in the presence of Au octahedral seeds and the capping agent hexadecyltrimethylammonium bromide (CTAB). Six syringes placed on six syringe pumps fed into PTFE tubing at the injector site through silica capillaries. The PTFE tubing was fed through an oil bath set at 25 °C so that room temperature fluctuations were accounted for during reactions. A total additive flowrate of 1.3 mL/hr for the reagent material was maintained for a residence time of 1.5 hours. The flow rates of syringe pumps 1 (Au precursor, CTAC, NaBr), 2 (Pd precursor, CTAC, NaBr), and 3 (HCl solution) were held equal or varied depending on the experiment. Syringe Pump 4 contained Au octahedral seeds (characterized in Figure S1) and was held constant at either 0.1 or 0.05 mL/hour. Syringe pump 5 contained L-aa and was held constant at 0.6 mL/hour. Syringe pump 6 contained the immiscible silicone oil and was held constant at 1.6 mL/hr. Full experimental details are in the ESI. Preliminary metal precursor concentration studies were undertaken to determine the starting concentrations in syringes 1 and 2. SEM images of the products can be found in Figure S2, with the highest metal precursor concentrations chosen for the flowrate manipulation study as this synthetic condition produced a high quality kinetic product, 8-branched Au-Pd nanocrystals with O_h symmetry. This product is anticipated based on previous reports of batch reaction SMCR producing octopodal AuPd nanostructures.[20]

By increasing the flowrate of the HCl solution in syringe 3 and decreasing to the flowrate of Au and Pd precursors in syringes 1 and 2 while holding the flowrate of seeded solution constant in syringe pump 4 at 0.1 mL/hr, morphological shape changes of the nanoproducts were observed (Figure 2, row 1). At relatively high pH, sharp octopods were produced. As the pH was lowered (increased HCl flow rate relative to metal precursors), blunt octopods, rounded octopods, polyhedra, and core@shell octahedra were synthesized, respectfully. As the HCl concentration increased with faster flowrates in the droplet reaction, the concentration of the metal precursors decreased with slower flowrates to maintain a total additive flowrate for syringes 1-4 of 0.7 mL/hr. By lowering metal precursor concentration in the reaction, smaller particles were synthesized. This size change is easily seen by comparing A1 and E1 products in Figure 2. The decrease in the pH allowed the products to change from branched to non-branched species through modifying growth kinetics. By adding more H^+

into the solution, L-aa stays in the protonated form. This modification changes the growth kinetics of the particle in solution, where the rate of adatom adsorption slows down with respect to adatom diffusion. By manipulating the adsorption rate with respect to the diffusion rate, the particle shape changes from kinetically favored sharp octopods to more stable core@shell octahedra, with different shapes in between.[33] The decrease in monodispersity from A1 to E1 could be attributed to atomic diffusion on the exterior of the particle, instead of instantaneous trapping at high energy sites such as in A1.

To account for the decrease of the metal precursor flowrates generating smaller particles, the Au seed flowrate in syringe 4 was halved to 0.05 mL/hr (generating less seeds in solution) allowing the flowrates of the metal precursors to be increased, maintaining the total additive flowrate of 0.7 mL/hr for syringe pumps 1-4. Products from this study are shown in Figure 2, row 2. The HCl flowrate for each reaction in row 2 corresponds to the HCl flowrate used in row 1 directly above. Changing the seed flowrate gives rise to new reagent ratios for row 2, while maintaining a similar pH as in row 1. Intuitively, less seeds and more metal precursors at a similar pH solution

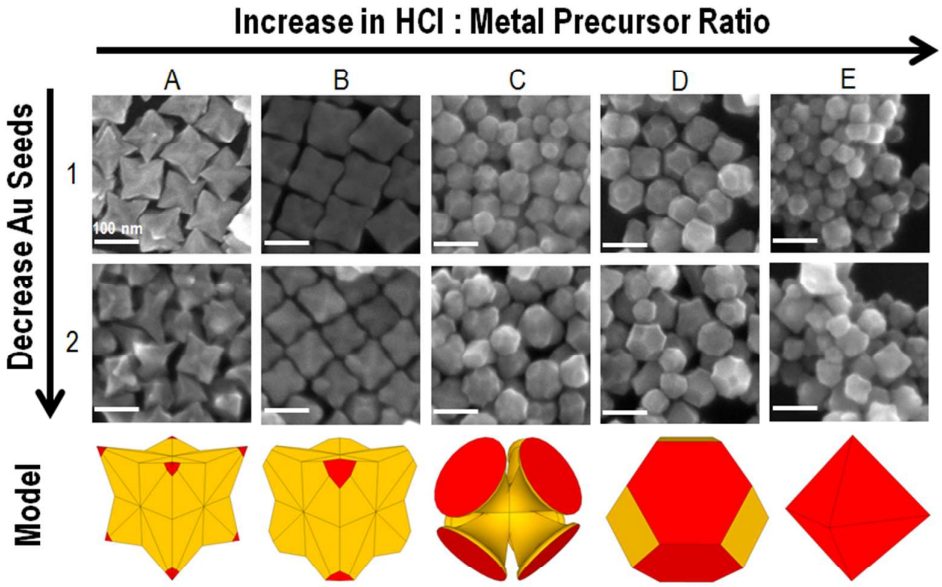

Figure 2. Flowrate study of SMCR syntheses in a microreactor. Kinetic products were synthesized by varying the relative flowrates of syringe pumps 1-4 keeping the additive total flowrate at 0.7 mL/hr. Left to right shows SEM images of the products synthesized by increasing the 250mM HCl flowrate with respect to the Au and Pd precursors. (row 1) The flowrate of the Au seed solution was constant at 0.1 mL/hr. (row 2) SEM images of the products synthesized by decreasing flowrate of the Au octahedral seed solution to 0.05 mL/hr. Models represent the particles shape and placement of atoms (Au=yellow, Pd=red).

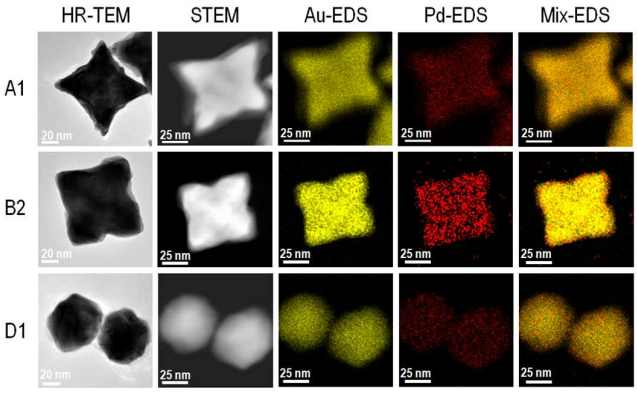

Figure 3. Detailed Analysis of three Au-Pd products shown in Figure 2 (A1= Sharp octopods, B2= Blunt Octopods, D1=Polyhedra). Elemental mapping shows the Au, Pd, and the overlay of both signals (Au=yellow, Pd=red).

should generate larger sized particles. This seed adaptation allowed for larger sized particles to be synthesized. This is specifically shown in the E1 and E2 case, but at the cost of monodispersity. However, this change was expected because the supersaturation of the metal precursors was significantly higher with respect to seed concentration when the seed flowrate was decreased. In other comparisons, the size differences were minimal and highlights how inline manipulation, rather than changing stock solutions or residence time, results in multiple synthetic variables changing simultaneously. Exact flowrate manipulations for rows 1 and 2 in Figure 2 for syringes 1-4 are outlined in Table S1. The flowrate of syringe pump 1 equaled the flowrate of syringe pump 2 in each synthesis.

To better characterize the NPs synthesized, three samples were selected for higher analysis. Products corresponding to A1, B2, and D1 in Figure 2 were selected. Figure 3 shows HR-TEM, STEM, and elemental mappings of

these samples. In each sample, Pd appears to be localized at the exterior, and for the branched species, it appears to predominantly be placed at the tips. These findings agree with the prior batch reactor reports.[20] STEM-EDS finds the Au:Pd atomic ratio of the A1, B2, and D1 to be 9:1, 7:1, and 9:1,with the diagonal lengths approximately 134.7 ± 10.6nm, 103.5 ± 6.3nm, and 83.8 ± 5.4nm, respectfully. We note that the Au:Pd atomic ratio is greater than the 5:1 input ratio of precursors as this measurement includes the Au from the seeds as well. In the A1 STEM image, the Au seed is visible but not as apparent in the B2 and D1 particles. As the HCl concentration was increased, the HR-TEM, STEM, and elemental mapping images show the overgrowth became more conformal, generating lower energy particles. This change in shape is due to adatoms having more time to diffuse and not become kinetically trapped. Absorbance measurements of A1, B2, and D1 can been seen in Figure S3. The absorbance blue shifts as the particles become polyhedral. PXRD patterns confirm a structure consisting of Au as well as a Au-rich Au-Pd alloy, consistent with the Au seeds and deposited Au-Pd alloy (Figure S4).

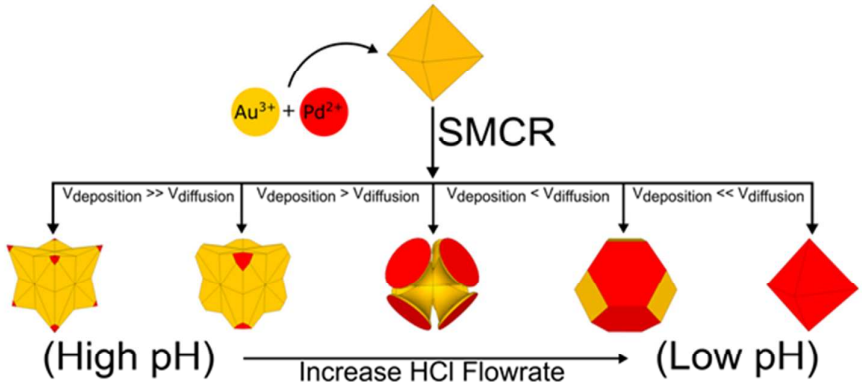

Scheme 1. Illustration of how pH tailors the rate of deposition with respect to rate of diffusion in SMCR, yielding Au-Pd NPs with different shapes (Au=yellow, Pd=red). The pH was adjusted inline through variation of the relative flowrates of reagent material.

Scheme 1 summarizes the effects of HCl in the microreactor droplets as a function of flowrate. As pH decreases, the rate of adatom diffusion increases with respect to the rate of adatom adsorption. This study shows that inline shape modification of NPs is possible and the products of the microreactor syntheses are comparable to products from batch reaction (Figure S5). In the absence of Au seeds, product uniformity cannot be achieved (Figure S6). By bridging the versatility of microreactors with the known synthetic routes of batch reactions, continuous flow production on nanomaterials is achievable.

Conclusions

We have shown that changing shape morphologies inline via a microreactor is possible by tailoring relative flowrates of reagents. A variety of kinetically controlled products, ranging from sharp octopods to lower energy core@shell octahedra, are accessible by incorporating HCl to change the growth modes of the NPs. By taking the versatility of microreactor synthesis and bridging it with known batch reactions, predictive continuous production of shape controlled complex NPs should be achievable.

This work was supported by NSF Award CHE-1602476. We thank IU's Electron Microscopy Center and Nanoscale Characterization Facility for access to instrumentation, and Dr. D. Morgan and A. Chen for their assistance with TEM.

Conflicts of interest

There are no conflicts to declare.

Notes and references

1 Y. Xia, Y. Xiong, B. Lim, and S. E. Skrabalak, *Angew. Chem. Int. Ed.*, 2009, **48**, 60-103.
2 X. Huang, S. Neretina, and M. A. El-Sayed, *Advanced Materials*, 2009, **21**, 4880-4910.
3 Z. Chen, X. Zhang, and G. Lu, *J. Phys. Chem. C*, 2017, **121**, 1964-1973.
4 E. C. Dreaden, M. A. Mackey, X. Huang, B. Kang, and M. A. El-Sayed, *Chem. Soc. Rev.*, 2011, **40**, 3391-3404.
5 K. A. Willets, and R. P. V. Duyne, *Annu. Rev. Phys. Chem.*, 2007, **58**, 267-297.
6 M. Shao, Q. Chang, J.-P. Dodelet, and R. Chenitz, *Chem. Rev.*, 2016, **116**, 3594-3657.
7 K. D. Gilroy, A. Ruditskiy, H-C. Peng, D. Qin, and Y. Xia, *Chem. Rev.*, 2016, **116**, 10414-10472.
8 E. Fantechi, A. G. Roca, B. Sepúlveda, P. Torruella, S. Estradé, F. Peiró, E. Coy, S. Jurga, N. G. Bastús, J. Nogués, and V. Puntes, *Chem. Mater.*, 2017, **29**, 4022-4035.
9 T.-H Yang, H.-C. Peng, S. Zhou, C.-T. Lee, S. Bao, Y.-H. Lee, J.-M. Wu, and Y. Xia, *Nano Lett.*, 2017, **17**, 334-340.
10 Y. Wang, H-C Peng, J. Liu, C. Z. Huang, and Y. Xia, *Nano Lett.*, 2015, **15**, 1445-1450.
11 X. Yin, M. Shi, J. Wu, Y.-T. Pan, D. L. Gray, J. A. Bertke, and H. Yang, *Nano Lett.*, 2017, **17**, 6146-6150.
12 F.-R. Fan, D.-Y. Liu, Y.-F. Wu, S. Duan, Z.-X. Xie, Z.-Y. Jiang, and Z.-Q. Tian, *J. Am. Chem. Soc.*, 2008, **130**, 6949-6951.
13 N. Ortiz, R. G. Weiner, and S. E. Skrabalak, *ACS Nano*, 2014, **8**, 12461-12467.

14 H. Zhang, M. Jin, J. Wang, M. J. Kim, D. Yang, and Y. Xia, *J. Am. Chem. Soc.*, 2011, **133**, 10422-10425.
15 Y. Xia, X. Xia, and H.-C. Peng, *J. Am. Chem. Soc.*, 2015, **137**, 7947-7966.
16 C. J. DeSantis, A. A. Peverly, D. G. Peters, and S. E. Skrabalak, *Nano Lett.*, 2011, **11**, 2164-2168.
17 C. J. DeSantis, A. C. Sue, A. Radmilovic, H. Liu, Y. B. Losovyj, and S. E. Skrabalak, *Nano Lett.*, 2014, **14**, 4145-4150.
18 M. R. Kunz, S. M. McClain, D. P. Chen, K. M. Koczkur, R. G. Weiner, and S. E. Skrabalak, *Nanoscale*, 2017, **9**, 7570-7576.
19 R. G. Weiner, and S. E. Skrabalak, *Chem. Mater.*, 2016, **28**, 4139-4142.
20 C. J. DeSantis, A. C. Sue, M. M. Bower, and S. E. Skrabalak, *ACS Nano* 2012, **6**, 2617-2628.
21 G. Niu, A. Ruditskiy, M. Vara, and Y. Xia, *Chem. Soc. Rev.*, 2015, **44**, 5806-20.
22 T. W. Phillips, I. G. Lignos, R. M. Maceiczyk, A. J. deMello, and J. C. deMello, *Lab Chip*, 2014, **14**, 3172-3180.
23 I. Lignos, R. Maceiczyk, and A. J. deMello, *Acc. Chem. Res.*, 2017, **50**, 1248-1257.
24 L. Zhang, G. Niu, N. Lu, J. Wang, L. Tong, L. Wang, M. J. Kim, Y. Xia, *Nano Lett.*, 2014, **14**, 6626-6631.
25 T. Gu, C. Zheng, F. He, Y. Zhang, S. A. Khan, and T. A. Hatton, *Lab Chip*, 2018, **18**, 1330-1340.
26 S. E. Skrabalak, and R. L. Brutchey, *Chem. Mater.*, 2016, **28**, 1003-1005.
27 L. J. Pan, J. W. Tu, H. T. Ma, Y. J. Yang, Z. Q. Tian, D. W. Pang, and Z. L. Zhang, *Lab Chip*, 2018, **18**, 41-56.
28 J. S. Santana, K. M. Koczkur, and S. E. Skrabalak, *Langmuir*, 2017, **33**, 6054-6061.
29 V. Sebastian, K. F. Jensen, *Nanoscale*, 2016, **8**, 15288-15295.
30 P. Kunal, E. J. Roberts, C. T. Riche, K. Jarvis, N. Malmstadt, R. L. Brutchey, S. M. Humphrey, *Chem. Mater.*, 2017, **29**, 4341-4350.
31 M. Shviro D. Zitoun, *RSC Adv.*, 2013, **3**, 1380-1387.
32 Y. H. Kim, L. Zhang, T. Yu, M. Jin, D. Qin, and Y. Xia, *Small.*, 2013, **9**, 3462-3467.
33 N. D. Burrows, S. Harvey, F. A. Idesis, and C. J. Murphy, *Langmuir*, 2017, **33**, 1891-1907.

TOC Figure: